Biosensors and Bioelectronics 26 (2010) 1593–1598

Contents lists available at ScienceDirect

Biosensors and Bioelectronics

journal homepage: www.elsevier.com/locate/bios

Differential spectral phase interferometry for wide dynamic range surface plasmon resonance biosensing

Siu-Pang Ng[a], Chi-Man Lawrence Wu[a,*], Shu-Yuen Wu[b], Ho-Pui Ho[b,**], S.K. Kong[c]

[a] Department of Physics and Materials Science, City University of Hong Kong, Hong Kong SAR, PR China
[b] Department of Electronic Engineering, The Chinese University of Hong Kong, Hong Kong SAR, PR China
[c] Department of Biochemistry, The Chinese University of Hong Kong, Hong Kong SAR, PR China

ARTICLE INFO

Article history:
Received 4 June 2010
Received in revised form 15 July 2010
Accepted 30 July 2010
Available online 12 August 2010

Keywords:
Surface plasmon resonance
Biosensor
Differential spectral interferometry

ABSTRACT

We introduce a novel wide dynamic range phase-sensitive surface plasmon resonance (SPR) biosensor based on differential spectral interferometry. Superseding conventional spectroscopic approach where only the SPR dip is monitored, our system acquires the spectral phase information of the entire electromagnetic field that undergoes SPR transformation. Since the SPR-induced phase change is highly wavelength specific with fixed incident angle, ultra-high sensitivity achievable through phase-sensitive detection, as reported herein, is maintained continuously across the spectral domain in response to refractive index changes. Our system has demonstrated a detection limit of 2.2×10^{-7} in terms of refractive index unit (RIU) using standard single-layer gold surface. In terms of biosensing performance, the estimated detection sensitivity obtained from bovine serum albumin (BSA) antibody–antigen binding experiments is 0.5 ng ml^{-1}.

1. Introduction

With rapid advancement over the last decade, surface plasmon resonance (SPR) biosensor has been indisputably recognized as the leading label-free sensing technique for bimolecular interaction analysis, pharmaceutical discovery and life science research (Prasad, 2003; Homola, 2008). SPR sensors utilize a confined electromagnetic wave known as surface plasmon propagating along the dielectric/metal interface as the sensing mechanism. Since the wave vector of such wave depends on the dielectric constants of both media, i.e. the dielectric sample and the metallic thin film, the confined surface plasmon is extremely sensitive to the alternation of dielectric constant in the vicinity of metallic surface. For excitation of the surface plasmon, Kretchmann prism coupling configuration is generally employed. The surface plasmon wave (SPW) vector (k_{sp}) is therefore matched by the tangential wave vector (k_x) of the p-polarized incident electromagnetic field. As the incident optical wave is polychromatic, the SPR coupling equation exhibit wavelength dependent characteristics, i.e.

$$k_{sp}(\lambda) = k_0(\lambda)\sqrt{\frac{\varepsilon_{sample}(\lambda)\varepsilon_{metal}(\lambda)}{\varepsilon_{metal}(\lambda)+\varepsilon_{sample}(\lambda)}} = k_0(\lambda)n_{prism}(\lambda)\sin\theta_{in} = k_x(\lambda), \quad (1.1)$$

where $k_0(\lambda)$ is the spectral free space wave vector, $\varepsilon_{metal}(\lambda)$ and $\varepsilon_{sample}(\lambda)$ are the wavelength dependent complex dielectric constants of the metal and the sample, respectively, $n_{prism}(\lambda)$ is the wavelength dependent refractive index of the prism coupler and θ_{in} is the angle of incidence. As a result, with certain dielectric property of the sample under test, an optimized wavelength exhibits maximum SPW coupling at appropriate angle of incidence. Therefore, a spectral dip is observed in the reflected spectrum and the corresponding reflection coefficients of the p- and s-polarized components (r_p and r_s) can be expressed as (Yeh, 1988)

$$\begin{cases} r_p(\lambda) = \sqrt{R_p(\lambda)}\exp[i\phi_p(\lambda)], \\ r_s(\lambda) = \sqrt{R_s(\lambda)}\exp[i\phi_s(\lambda)]. \end{cases} \quad (1.2)$$

Since the p-polarized phase angle $\phi_p(\lambda)$ demonstrates a large change at the resonant peak, a small change of $\varepsilon_{sample}(\lambda)$ will lead to a significant change of $\phi_p(\lambda)$ and accompanied by the differential phase $\Delta\phi(\lambda) = \phi_p(\lambda) - \phi_s(\lambda)$ (Wu et al., 2004).

However, the optical oscillation in Eq. (1.2) is too fast to be detected directly by any electronic detectors, thus conventional spectrometer only measures the power spectrum of SPR reflection, i.e. $R_p = |r_p(\lambda)|^2$, whereas the phase information $\phi_p(\lambda)$ is completely lost. In addition, optimized SPW coupling always leads to significant reduction of signal-to-noise ratio at the optimal wavelength, hence the spectrometer receives limited optical signal at the spectral dip which is overwhelmed by the shot-noise of the photo-detector. Therefore, it is quite challenging to determine the exact position of the dip. Due to these drawbacks, detection limit of conventional spectroscopic SPR devices is usually 10^{-5} in terms of refractive

* Corresponding author: Tel.: +852 3442 8668; fax: +852 3442 0538.
** Corresponding author: Tel: +852 2609 8279; fax +852 2603 5558.
E-mail addresses: lawrence.wu@cityu.edu.hk (C.-M.L. Wu), hpho@ee.cuhk.edu.hk (H.-P. Ho).

0956-5663/$ – see front matter © 2010 Elsevier B.V. All rights reserved.
doi:10.1016/j.bios.2010.07.128

index unit, which corresponds to 1 pg mm^{-2} of the biomaterial accumulated at the biosensing surface (Ho et al., 2001; Frischeisen et al., 2008).

In order to resolve the sensitivity issue, phase interrogation schemes was first introduced by means of optical heterodyning (Nelson et al., 1996). As a result, interferometric technique which is extremely popular for optical phase detection was adopted to improve the sensitivity limit of SPR devices. Several recent studies have demonstrated that it could be enhance by at least two order of magnitude by adopting the phase detection scheme (Kabashin and Nikitin, 1998; Wu et al., 2004; Chiang et al., 2005; Naraoka and Kajikawa, 2005; Su et al., 2005; Ho et al., 2006; Kabashin et al., 2009). However, due to the resonance nature of the SPR effect, the phase angle changes non-linearly as the refractive index shifts away from the optimal wavelength. It is due to the fact that the maximum slope of the phase curve always coincides with the resonance dip, thus leading to a large change of phase angle by a small alternation of sample refractive index. However, as the refractive index continues to change, the phase angle quickly saturates, hence forcing a compromise between sensitivity and dynamic range of phase measurements.

Our system is based on differential spectral interferometry where the SPR phases of p- and s-polarized components are simultaneously acquired from the visible-to-near infrared spectrum. The wavelength-dependent optical path difference (OPD) introduced between the reference and probing arms of the Michelson interferometer generates spectral oscillations that carry the important phase information, i.e. amplitude and phase of the entire electromagnetic spectrum undergoing SPR transformation. As the refractive index changes, the maximum SPR-induced phase shift is continuously monitored over the acquired spectrum despite the shifts in optimal SPR coupling from one wavelength to another. Since SPR only affects the p-polarized component, the s-polarized spectral fringe serves as the real-time reference. By mutual subtraction of the p- and s-polarized phase data, the SPR-induced differential phase information can be readily extracted from every spectral component. Another advantage of employing spectral phase interferometry is that temporal phase modulation which is essential for other wide dynamic SPR phase sensing scheme (Markowicz et al., 2007; Law et al., 2007) is no longer necessary, thus leading to improved real-time biosensing performance. In other words, by having an interferometer within the spectral SPR sensing scheme, we have effectively combined the most desirable features of phase-sensitive and spectral SPR techniques. To demonstrate the two important characteristics of our system: wide dynamic range and high sensitivity of RIU based biosensing, two quantitative studies are included: (1) SPR phase measurement of sodium chloride (NaCl) solutions of various concentrations, (2) binding reaction between bovine serum albumin (BSA) and BSA antibodies of different concentrations.

2. Theoretical analysis

The theoretical analysis of spectral interferometry can be considered as the mutual interference of two beams from a white light source at the exit of the Michelson interferometer. Assuming the interference is detected at a transverse position vector $\mathbf{r}$, the resultant spectral power density $S(\mathbf{r},\omega)$ depends on the optical angular frequency ω as stated by the spectral interference law (Mandel and Wolf, 1995)

$$S(\mathbf{r},\omega) = S_1(\mathbf{r},\omega)+S_2(\mathbf{r},\omega)+2\sqrt{S_1(\mathbf{r},\omega)S_2(\mathbf{r},\omega)}\cos\left[\frac{\omega}{c}\Delta(\mathbf{r},\omega)\right], \quad (2.1)$$

where $S_1(\mathbf{r},\omega)$ and $S_2(\mathbf{r},\omega)$ are the spectral densities of the reference and probe beams, respectively, c is the speed of light, and $\Delta(\mathbf{r},\omega)$ is the spatially and spectrally dependent overall OPD between the reference and probe beams. Integrating over the optical aperture before entering the spectrometer, the resultant spectral power $P(\omega)$ becomes

$$P(\omega) = P_1(\omega)+P_2(\omega)+2V_A(\omega)\sqrt{P_1(\omega)P_2(\omega)}\cos\left[\frac{\omega}{c}\Delta(\omega)\right], \quad (2.2)$$

where $V_A(\omega)$ is the wavelength-dependent fringes visibility after the aperture. The recorded spectral intensity $I(\omega)$ can be expressed by the convolution between the spectral power function $P(\omega)$ and the spectrometer response function $R(\Delta\omega)$ such as (Hlubina, 2004)

$$I(\omega) = I_1(\omega)+I_2(\omega)+2V_A(\omega)V_R(\omega)\sqrt{I_1(\omega)I_2(\omega)}\cos[\phi_R(\omega)], \quad (2.3)$$

where $V_R(\omega)$ is the wavelength-dependent fringes visibility resolved by the spectrometer and $\phi_R(\omega)$ is the spectral phase. Taking into account of the SPR effect and assuming our interferometer is well compensated, i.e. the second-order dispersion is negligible, the above expression can be converted into functions of the wavelength λ and separated for respective p- and s-polarizations

$$\begin{cases} I_p(\lambda) = I_0(\lambda)\left\{1+V_p(\lambda)\cos[\phi_{OPD}(\lambda)+\phi_p(\lambda)+\phi_{noise}]\right\}, \\ I_s(\lambda) = I_0(\lambda)\left\{1+V_s(\lambda)\cos[\phi_{OPD}(\lambda)+\phi_s(\lambda)+\phi_{noise}]\right\}, \end{cases} \quad (2.4)$$

where $I_0(\lambda)$ is the reference spectrum, $V_{p,s}(\lambda)$ is the simplified spectral fringe visibility term due to SPR reflectivity $r_{p,s}(\lambda)$, $\phi_{OPD}(\lambda)$ is the OPD introduced between the two interferometric arms, and the subscripts *p*, *s*, and *noise* carry their respective definitions. Since we are only interested with the SPR induced phase retardation, i.e. $\phi_p(\lambda)$ and the s-polarized phase $\phi_s(\lambda)$ is known to remain unchanged, the wavelength specific SPR differential phase $\Delta\phi(\lambda)=\phi_p(\lambda)-\phi_s(\lambda)$ can be extracted by mutual subtraction of the two phase terms of Eq. (2.4). Also, it should be noted that our spectral Michelson interferometer enjoys the same phase amplification as that reported by past investigators (Yuan et al., 2007) as the p-polarized probe beam traverses the SPR cell twice.

Our numerical analysis of the spectral SPR phase response with a 48 nm thick gold layer and NaCl solution of various concentrations as illuminated by the warm white LED source are shown in Fig. 1a and b. Here we demonstrate the spectral phase sensitivity for narrow and wide range of refractive index change. It is obvious for narrow range of RIU, the spectral phase performs similarly to laser interferometry, i.e. minuscule RIU changes are accompanied by large phase jump at a single wavelength; as the RIU increases, the initial phase response starts to saturate as the optimal SPW coupling wavelength shifts, thus the phase response is highly wavelength specific as the angle of incidence remains unchanged at 70°. With spectral phase interferometry, it is possible to follow the best phase response across the acquired spectrum so the wide dynamic measurement range is realized without sacrificing the ultra-high phase sensitivity. This is impossible for conventional laser based SPR phase sensing systems. In addition, no temporal phase modulation is necessary as the SPR phase is acquired directly from the spectral domain, which greatly simplified the operation of our system.

3. Experimental details

3.1. Materials

Commercially available chemicals were used as received. For the measurement of refractive index change, sodium chloride solutions of various concentrations were prepared from product of Fisher Scientific (www.fishersci.com). Phosphate buffered saline (PBS) was obtained from Invitrogen (www.invitrogen.com). BSA and anti-BSA samples were obtained from Sigma–Aldrich (www.sigmaaldrich.com).

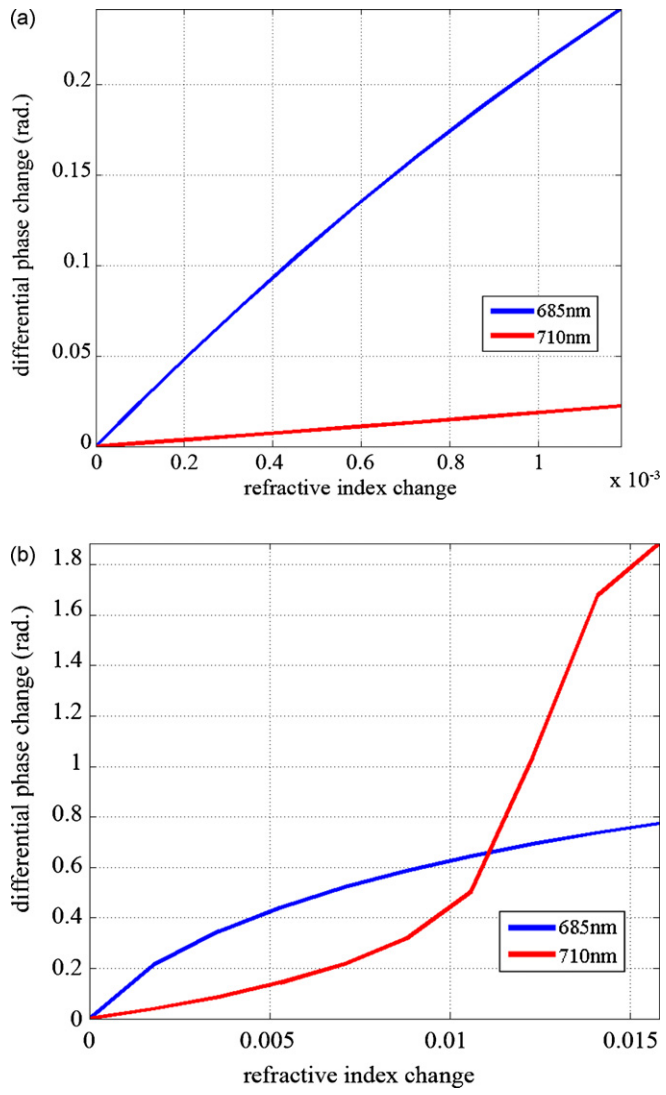

Fig. 1. Differential phase change of two wavelengths: (a) a narrow range of refractive index change and (b) a wide range of refractive index change.

3.2. SPR spectral interferometer

A schematic diagram of our differential spectral interferometer for SPR phase sensing is shown in Fig. 2. A 40 W warm white light emitting diode (LedEngin, www.ledengin.com) with central wavelength at 600 nm and full-width-half-maximum (FWHM) of 160 nm ranged from 520 to 680 nm was employed as the high power white-light source. A fiber coupled collimator (Thorlabs, www.thorlabs.com) was used to direct a parallel beam through a Glan-Thomson broadband linear polarizer (Edmund Optics, www.edmundoptics.com) at 45° before entering the Michelson interferometer. Two pieces of high tolerance right-angle prisms made of BK7 glass (Edmund Optics) were employed as the SPR couplers. Glass slides (Fisher Scientific) with 48 nm nominal thick gold coating were utilized as the sensing surface. The slides were attached to the prisms with refractive index matching oil (Cargille 11510, www.cargille.com). A customized Teflon™ (DuPont, www.dupont.com) flow chamber was brought into contact with the gold film and the estimated sensing area was about 10 mm^2 in the probe cell. The reference cell contains exactly the same components except that the flow chamber remains empty and thermally stabilized throughout the experiment. There are two reasons for incorporating the reference cell: (1) the spectral interferometer is essentially comparing the refractive indices in the two optical paths, one of them must remains unchanged so that the RIU change in the probe path can be determined; (2) the optical property of BK7 prism is different from air, so dispersion is unavoidable and deters spectral fringe visibility, therefore the reference cell is necessary to compensate the dispersion caused by the probe cell. Two high precision 1/20 lambda mirrors (Edmund Optics) were placed at respective ends of the optical paths. One of the mirrors was mounted on a linear translation stage for OPD adjustment. The Wollaston prism (United Crystal, www.unitedcrystals.com) was inserted at the exit of the interferometer, so the p- and s-polarized components were separated into the dual channel spectrometer (AvaSpec3648, www.avantes.com). The spectral oscillations were transferred into the personal computer for differential phase processing via MATLAB™ (www.mathworks.com) routines.

3.3. Sample preparations and measurement

Sodium chloride solutions of 0.5%, 1%, 2%, 4%, 6%, 8%, 10% and 10.5% were prepared by mixing appropriate weights of crystalline salt with purified de-ionized water. The solutions were kept in sealed bottles and stored in the same enclosed chamber with the interferometer for 24 h before the experiment. The adsorption monolayer of BSA was first immobilized on the gold surface by the following steps: (1) the sensor chips was incubated in 10 mM of 11-mercaptoundecanoic acid (MUA) for at least 4 h, (2) the chips was then removed and further incubated in 0.4 M 1-ethyl-3-(3-dimethylaminopropyl) carbodiimide hydrochloride (EDC)/N-hydroxysuccinimide 0.15 M (NHS) solution for at least 10 min, (3) 1 mg ml^{-1} BSA was then added onto the prepared chip surface for at least 10 min, (4) 1 M ethanolamine solution was added onto the gold surface and incubate for 10 min, (5) the chips was then washed with PBS buffer solution, (6) Assuming that a BSA monolayer has been formed, the chips were then kept in PBS solution and stored at 4 °C until the experiment. As the anti-BSA was received in resin form with concentration of 2 mg ml^{-1}, we diluted it to 20 μg ml^{-1} and 2 μg ml^{-1}. Assuming that the molecular weight of anti-BSA is 150 kDa, the two concentrations corresponded to 0.13 μM and 13 Nm, respectively. The diluted anti-BSA samples were frozen at −18 °C before experiment.

Calibration of the system was performed by flowing purified de-ionized water then prepared sodium chloride solutions over the gold film in the probe cell. The corresponding refractive index range was approximately 1.3333–1.3505 RIU (Weast, 1983) and the RIU changed from 9×10^{-4} to 1.72×10^{-2} covering more than two orders of magnitude. The interferometer was sealed in an enclosed polystyrene chamber on top of a floated optical table to ensure minimum thermal and mechanical disturbance from the surrounding. To monitor the experimental fluctuation, purified de-ionized water was injected into the probe cell and the spectral phase is continuously measured over a period of 30 min. The experimental phase fluctuation was found to be 2×10^{-4} rad (approximately 0.01°). For biosensing of BSA–anti-BSA interaction, PBS buffer was first injected into the flow cell to remove excessive BSA on the gold layer; anti-BSA samples were then injected into the flow cell and left for one and a half hour to allow sufficient time for complete antigen–antibody interaction. At the end of the experiment, the flow cell was flushed with PBS buffer again. All detection experiments were repeated at least twice to ensure acceptable level of consistency of our data.

4. Results and discussion

The differential spectral phase as a function of wavelength and against various sodium chloride concentrations are shown in Fig. 3a

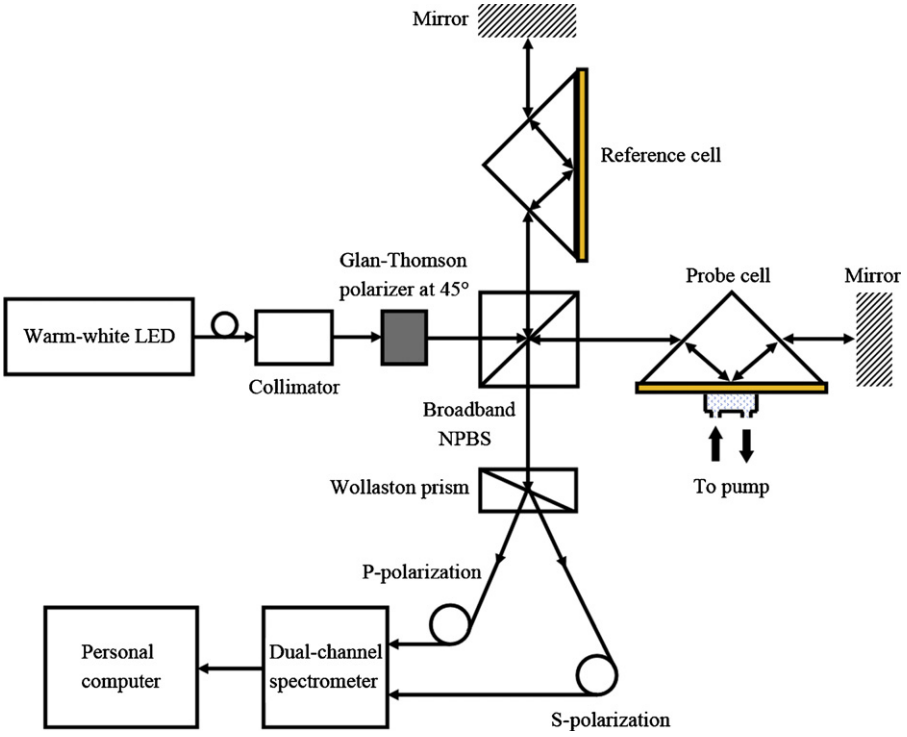

Fig. 2. Schematic configuration of the differential spectral interferometer, NPBS stands for non-polarizing beam splitter.

and b, respectively. Our experimental result in Fig. 3b showed that a change in refractive index of 8×10^{-4} RIU (0.5% NaCl to 1% NaCl) led to 0.6283 rad phase change at about 646.2 nm. With 2×10^{-4} rad phase fluctuation, it corresponds to a resolution (detection limit) of 2.2×10^{-7} RIU, which is about the same level of existing systems which employed standard gold film as the sensing layer (Markowicz et al., 2007; Law et al., 2007; Yuan et al., 2007). At low concentrations, it is obvious that SPR-induced phase jump occurs at around 646.2 nm and the resolution of 2.2×10^{-7} RIU is only attainable around this optimal wavelength, whereas the phase slopes of other wavelengths remain almost horizontal which indicates the optimal phase sensitivity is highly wavelength specific and this observation agrees with our simulation. As the concentration increases, the optimal SPW coupling shifts to longer wavelengths. Therefore, the phase of the original wavelength 646.2 nm starts to saturate as its phase slope becomes horizontal and the detection limit drops to 1.1×10^{-6} RIU (2% NaCl to 4% NaCl). Fortunately, as we are monitoring the spectral phases of the spectrum over a large range of wavelengths, the optimal phase jump is continuously pursued across the acquired spectrum. As indicated in Fig. 3b, at the wavelength of 646.2 nm, the maximum sensitivity of 2.2×10^{-7} RIU occurs between 0.5% and 1% sodium chloride concentrations; for 653.7 nm, the maximum sensitivity is attained between concentrations of 2% and 6%; as for 664.3 nm, the maximum sensitivity can be achieved with concentrations over 8–10%. Thus it is obvious that the occurrence of maximum sensitivity changes as the analyte concentration varies. So a monochromatic laser would not be ideal to test analyte with a range of concentrations as the sensitivity varies and so the interpreted result may not be adequately reliable. We should also point out that the current so-called "wide dynamic range" is essentially confined to the context of overcoming drawback of previous fixed incident angle SPR phase measurement technique which is well-known for its narrow dynamic range despite its prevailing detection limit.

To further demonstrate the real-time refractive index sensing capability of our system, 2% sodium chloride solution by weight was injected into the purified water containing probe cell for duration of 200 s and then the sensing chamber was re-flushed with purified water for another 200 s and finally refilled with 2% sodium chloride. Fig. 4 is the 2D plot of the wrapped spectral phase (scale shown on the color bar) obtained from the p-polarized channel. For the first 170 s, the chamber contained only purified water and since the system was thermally stabilized and the pump was off, spectral phase drift was negligible which indicated the system was ready for operation. Between the 170th second to 180th second, 2% sodium chloride solution was pumped into the sensing cell and at the end of the 180th second the pump was switched off. The spectral fringe at 654.3 nm has significantly large phase jumps upon the sudden change of refractive index resulting from the sodium chloride injection, as shown in Fig. 4. This was maintained for 150 s. After this, the sensing cell was re-flushed with purified water at the 330th second. It is obvious that the spectral peak has disappeared, and the spectral phase of this particular wavelength has recovered its initial level. Another observation is that our interferometric system was well stabilized. This is because when there is no RIU change at the sensing surface, the spectral phase remained almost stationary, which is a strong support of the claimed 10^{-4} rad stability essential for ultra sensitive RIU detection. For further illustration of the highly wavelength specific spectral phase shift, we extract spectral phase variations of two different wavelengths over the entire process from Fig. 4 then differentiate with respective s-polarizations and plot the phase differences in Fig. 5. It is reminded that at the 170th second, the probe cell was filled with 2% sodium chloride solution and at the 330th second it was flushed with purified water. The raw fringe was first filtered with fast Fourier transform (FFT) routine to remove the zero order non-modulating components then inverted back to the spectral domain. Subsequence spectral fringe was processed by windowed Fourier filtering (WFF) technique (Qian et al., 2008; Hlubina et al., 2008) to extract the spectral phase from respective polarization channels. It is obvious that at the optimal wavelength of 654.3 nm, phase shifted significantly for almost π radian, whereas the phase change of the non-optimized wave-

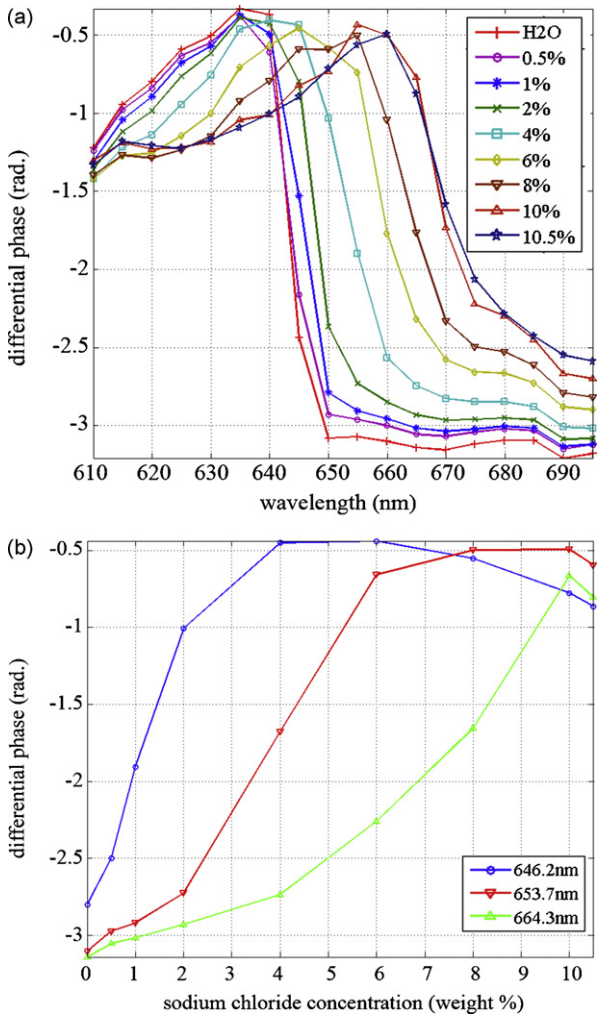

Fig. 3. (a) Differential phase vs. wavelength of various sodium chloride concentrations. (b) Differential phase vs. refractive index of three selected wavelengths.

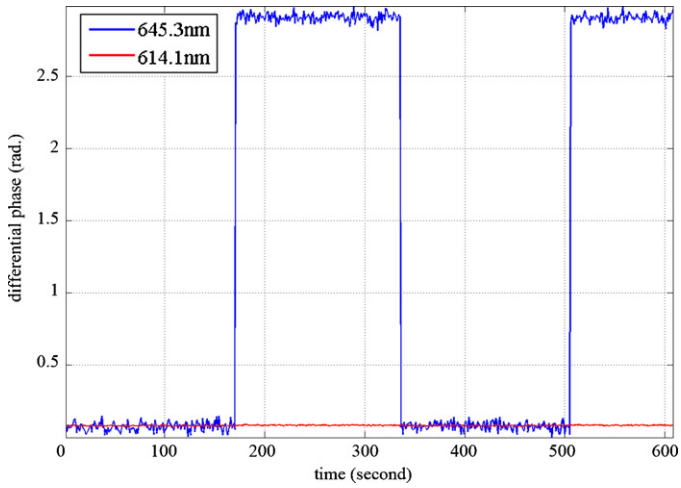

Fig. 5. Differential phase shift of selected wavelength 645.3 nm and 614.1 nm.

length 614.1 nm is virtually zero. With the stability of 10^{-4} rad, we have again achieved an estimated detection limit in the range of 10^{-7} RIU for real-time monitoring.

For biosensing applications, the sensor chips incubated with BSA monolayer were retrieved from the refrigerator and rested at room temperature for 30 min before installing into the probe cell. Similarly the anti-BSA reagent was retrieved from the freezer and brought to room temperature before testing. PBS solution was first flushed into the probe cell to remove excessive BSA which was not bonded to the gold surface. The PBS buffer was retained in the flow cell for one and a half hour and the spectral phases were continuously recorded. This serves as a control experiment as the anti-BSA concentration in this case is zero. The inset of Fig. 6 shows the phase fluctuation over the entire period, and the standard deviation of the fluctuation was found to be 2×10^{-4} rad. This value can be subsequently translated into the limit of detection of the system. After that, anti-BSA of 20 $\mu g\,ml^{-1}$ and 2 $\mu g\,ml^{-1}$ were injected into the probe cell in separate trials. The spectral fringes were continuously recorded for 5000 s. Finally the probe cell was flushed with PBS to ensure that free anti-BSA, if any, would be washed away. The fringes were treated in a similar fashion as mentioned earlier and the dif-

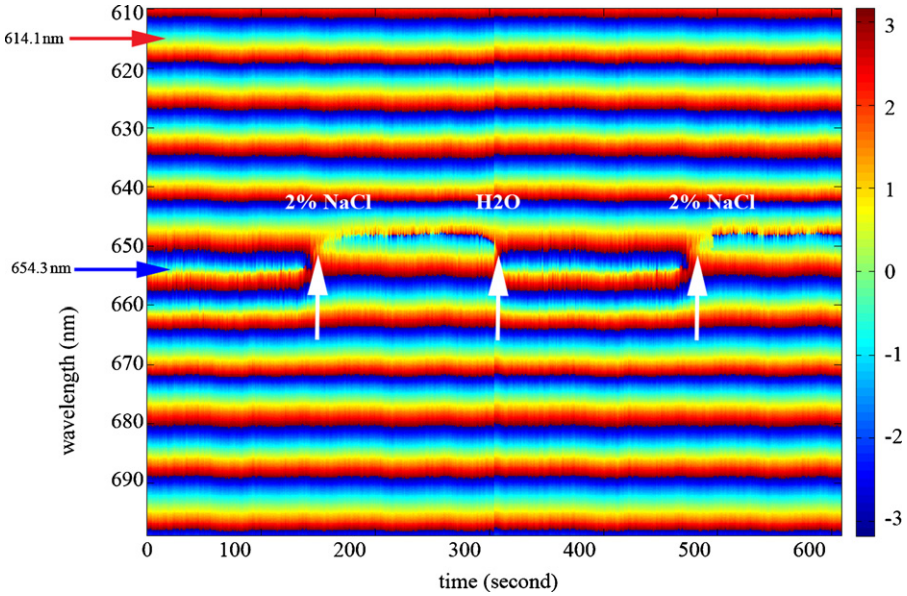

Fig. 4. Spectral phase of p-polarization over a long period with injection of 2% sodium chloride and flushing with water at different instances.

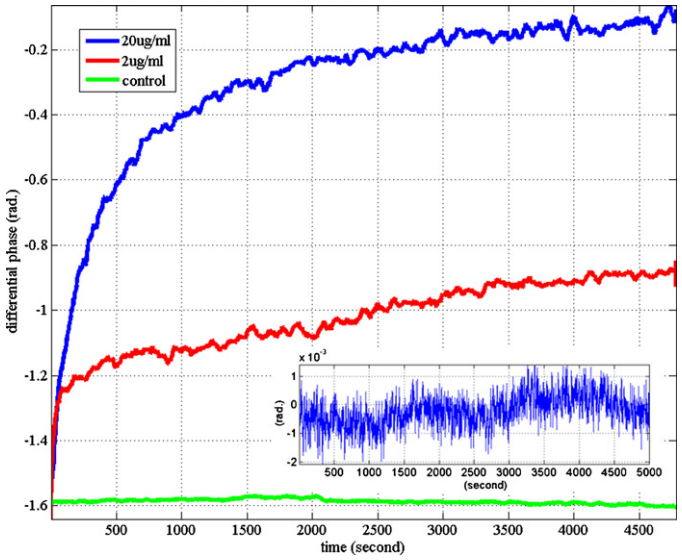

Fig. 6. Phase response curve obtained from BSA–anti-BSA interaction of 646.5 nm and the control phase plot obtained from 605 nm. Inset of Fig. 6 corresponds to the 646.5 nm phase fluctuation with PSB buffer in a period of 5000 s.

ferential phases were obtained by mutual subtraction of the p- and s-polarization components at every instance. Fig. 6 shows our result for the two different concentrations of a selected wavelength (i.e. 646.5 nm) and the phase of a non-SPW coupling wavelength (i.e. 605 nm) as the real-time reference. With the first case of 20 μg ml^{-1} anti-BSA, the total of 1.53 rad phase shift was observed. Given that the phase fluctuation has a standard deviation of 2×10^{-4} rad, a linear extrapolation of 1.53 rad phase change from the 20 μg ml^{-1} sample corresponds to a detection limit of 2.2 ng ml^{-1}. For the case of 2 μg ml^{-1}, the total phase change was 0.76 rad. With the same phase fluctuation, the detection limit is 0.5 ng ml^{-1}, which is comparable to the best reported in literature (Homola, 2008; Fan et al., 2008). The different detection limits obtained from the two experiments can be explained by a non-linear behaviour of the SPR phase response curve. For example, as shown in Fig. 3b, depending on the choice of wavelength and starting refractive index value, linear behaviour occurs only when the total phase change is somewhere between 1 and 2 rad. For the case of 20 μg ml^{-1}, a total phase change of 1.53 rad is very likely to have exceeded the linear region, thus leading to a less favourable detection performance. On the other hand, the lower concentration case of 2 μg ml^{-1} should be well within the linear region where the slope is much larger. Consequently an experimental detection limit of 0.5 ng ml^{-1} for this case can be justified. This has also indicated that an improvement is necessary to represent the overall spectral phase change with moderate to large RIU variations. To this end, a phase tracking algorithm is currently under investigation.

5. Conclusions

We have presented a novel fixed angle phase-sensitive surface plasmon resonance biosensor which has both wide dynamic range and high detection sensitivity. To the best of our knowledge, this is the first time that such a direct approach for achieving wide dynamic range and high sensitivity through combining phase-sensitive and spectral interrogations. The scheme employs a high power warm-white LED source with differential spectral interferometry which the SPR phase information is directly acquired from the spectral domain. We have experimentally demonstrated the wide dynamic range with sodium chloride solution of various concentrations and the detection limit is estimated to be 2.2×10^{-7} in terms of refractive index unit (RIU). We have also successfully applied the proposed system in bio-sensing of BSA anti-BSA interaction and the detection limit is estimated to be 0.5 ng ml^{-1}, which is comparable with the best detection limit reported in the literature. Further enhancement such as the implementation of low-loss long range surface plasmon resonance (LRSPR) to improve the detection limit is currently undertaken.

Acknowledgements

The authors wish to thank the Research Grant Council for providing funding support under project #411208. A research studentship (Siu-Pang Ng) provided by City University of Hong Kong is also gratefully acknowledged.

References

Chiang, H.P., Lin, J.L., Chang, R., Su, S.Y., Leung, P.T., 2005. Opt. Lett. 30, 2727–2729.
Fan, X.F., White, I.M., Shopova, S.I., Zhu, H.Y., Suter, J.D., Sun, Y.Z., 2008. Anal. Chim. Acta 620, 8–26.
Frischeisen, J., Mayr, C., Reinke, N.A., Nowy, S., Brutting, W., 2008. Opt. Express 16, 18426–18436.
Hlubina, P., 2004. J. Mod. Opt. 51, 537–547.
Hlubina, P., Lunacek, J., Ciprian, D., Chlebus, R., 2008. Opt. Commun. 281, 2349–2354.
Ho, H.P., Wu, S.Y., Yang, M., Cheung, A.C., 2001. Sensors Actuat. B: Chem. 80, 89–94.
Ho, H.P., Law, W.C., Wu, S.Y., Liu, X.H., Wong, S.P., Lin, C., Kong, S.K., 2006. Sens. Actuators B 114, 80–84.
Homola, J., 2008. Chem. Rev. 108, 462–493.
Kabashin, A.V., Nikitin, P.I., 1998. Opt. Commun. 150, 5–8.
Kabashin, A.V., Patskovsky, S., Grigorenko, A.N., 2009. Opt. Express 17, 21191–21204.
Law, W.C., Markowicz, P., Yong, K.T., Roy, I., Baev, A., Patskovsky, S., Kabashin, A.V., Ho, H.P., Prasad, P., 2007. Biosens. Bioelectron. 23, 627–632.
Mandel, L., Wolf, E., 1995. Optical Coherent and Quantum Optics. Cambridge University Press, New York.
Markowicz, P., Law, W.C., Baev, A., Prasad, P., Patskovsky, S., Kabashin, A.V., 2007. Opt. Express 15, 1745–1754.
Naraoka, R., Kajikawa, K., 2005. Sens. Actuators B 107, 952–956.
Nelson, S.G., Johnston, K.S., Yee, S.S., 1996. Sensors Actuat. B: Chem. 35–36, 187–191.
Prasad, P.N., 2003. Introduction to Biophotonics. Wiley-Interscience.
Qian, K., Wang, H., Gao, W., 2008. Appl. Opt. 47, 5408–5419.
Su, Y.D., Chen, S.J., Yeh, T.L., 2005. Opt. Lett. 30, 1488–1490.
Weast, R.C., 1983. CRC Handbook of Chemistry and Physics, 64th ed. CRC Press.
Wu, S.Y., Ho, H.P., Law, W.C., Lin, C., Kong, S.K., 2004. Opt. Lett. 29, 2378–2380.
Yeh, P.C., 1988. Optical Waves in Layered Media. Wiley.
Yuan, W., Ho, H.P., Wong, C.L., Kong, S.K., Lin, C., 2007. IEEE Sens. J. 7, 70–73.